AIChE Journal
DOI 10.1002/aic.15095

Accepted Article

Probing Pore Blocking Effects on Multiphase Reactions within Porous Catalyst Particles Using a Discrete Model

Guanghua Ye [a, b], Xinggui Zhou [a, *], Marc-Olivier Coppens [b, †], Weikang Yuan [a]

[a] State Key Laboratory of Chemical Engineering, East China University of Science and Technology, Shanghai 200237, China

[b] Department of Chemical Engineering, University College London, London WC1E 7JE, UK

[*] First corresponding author. Tel.: +86-21-64253509. Fax.: +86-21-64253528. Email address: xgzhou@ecust.edu.cn

[†] Second corresponding author. Tel.: +44-20-31081126. Fax.: +44-20-73832348. Email address: m.coppens@ucl.ac.uk

This article has been accepted for publication and undergone full peer review but has not been through the copyediting, typesetting, pagination and proofreading process which may lead to differences between this version and the Version of Record. Please cite this article as doi: 10.1002/aic.15095
© 2015 American Institute of Chemical Engineers (AIChE)
Received: Aug 13, 2015; Revised: Oct 26, 2015; Accepted: Oct 30, 2015

This article is protected by copyright. All rights reserved.

Accepted Article

Abstract

A discrete model coupling mass transfer, reaction, and phase change in porous catalyst particles is proposed to probe pore blocking effects on multiphase reactions. This discrete model is validated by comparing the results with experiments and those obtained using a continuum model, for the hydrogenation of benzene to cyclohexane in Pd/γ-alumina catalyst particles. The results show that pore blocking has a significant effect on the effectiveness factor and can contribute to up to 50% of the hysteresis loop area for multiphase reactions in porous catalysts, indicating that pore blocking must be accounted for. Moreover, the pore blocking effects are significantly enhanced when the pore network is poorly connected and the pore size distribution is wide, while the pore blocking effects are insensitive to the volume-averaged pore size. Multiphase catalyst material characterization and design should account for this effect.

Keywords: *pore network, discrete model, pore blocking, multiphase reactions, hysteresis, hydrogenation of benzene to cyclohexane*

This article is protected by copyright. All rights reserved.

Accepted Article

Introduction

Multiphase reactions, including various hydrotreating reactions, are of great importance in the refining and chemical industries. Many such reactions are catalyzed by porous catalysts. For example, Pd/γ-alumina is used to catalyze the hydrogenation of benzene to cyclohexane. In these catalyst particles, mass transfer, reaction and phase change can occur simultaneously. Due to this complexity, the apparent reaction rates, which differ from intrinsic rates, can be significantly affected by reaction conditions and become very difficult to predict. A better understanding of multiphase reactions in porous catalysts is still needed to design these catalysts, as well as gas/liquid/solid reactors.

In numerous multiphase reaction experiments conducted at the particle level,[1-4] inconsistent steady state branches were found as reaction conditions were changed in different directions, forming hysteresis loops when plotting reaction rate or effectiveness factor as a function of the control variable. The root cause of this hysteresis is believed to be inconsistent degrees of wetting in catalyst particles between a condensation process and an evaporation process.[3,5] Behind this inconsistency, there are two main reasons according to the literature on adsorption/desorption hysteresis.[6,7] One is the difference between the contact angles of condensing liquid and evaporating liquid, resulting in different critical pore radii for capillary condensation. The other one, which was occasionally mentioned but not investigated in literature on multiphase reactions, is pore blocking.

Pore blocking is very common in processes involving phase changes in mesoporous media, e.g., N_2 adsorption/desorption at low temperature and various multiphase reactions. In these processes, the liquid in some broad pores, which is supposed to have evaporated, can be blocked by the liquid in neighboring pores, as shown in Fig. 2. The pore blocking effects on adsorption/desorption hysteresis have been widely investigated.[8-12] The pore blocking effects can

This article is protected by copyright. All rights reserved.

Accepted Article

be very strong, resulting in a sharp desorption knee; more interestingly, the pore blocking effects can be significantly strengthened or weakened by the pore structure, e.g., connectivity and pore size distribution. But, to the best of our knowledge, the pore blocking effects on hysteresis in reaction rate and associated effectiveness factor have not been reported up to now. To carry out such a study, a proper model, which is able to describe the pore blocking phenomena, must be proposed.

Some continuum models have been used to simulate the coupled mass transfer, reaction, and phase change in partially wetted catalysts.[1,4,5,13,14] These models are reasonable approximations in certain cases where pores are well connected and local heterogeneities can be neglected. For numerous porous media, the limited pore connectivity and local heterogeneities, however, affect mass transfer and pore blocking to a large extent. Most importantly, using these models, one cannot detect the blocked liquid in large pores that is supposed to have evaporated but is trapped by the liquid in their adjacent pores. Considering this, a discrete model is an excellent alternative.

Examples of discrete pore models include Bethe lattices and pore networks, which were summarized by Sahimi et al.[15] and Keil[16]. Discrete models are advantageous in many respects,[16] e.g., (1) the connectivity is accounted for, (2) local heterogeneities can be included, (3) the pore wall can be smooth, irregular or even fractal,[17,18] and (4) fitting parameters like tortuosity can be avoided. Most importantly, pore blocking can be included in a discrete model. Due to these advantages, discrete models are widely used in simulating reaction, drying and multiphase flow processes in porous media. Early attempts have been made to simulate multiphase reactions in porous catalyst particles using a discrete model,[19,20] in which diffusion and reaction, however, are assumed to only occur in the vapor phase. Up to now, the discrete approach has not been employed to simulate hysteresis phenomena in any multiphase reaction systems.

This article is protected by copyright. All rights reserved.

Accepted Article

Hydrogenation of benzene to cyclohexane is an appropriate model reaction system for investigation, because of its industrial and academic importance. The kinetics of this reaction in Pd/γ-alumina catalysts has been well studied by Zhou et al.[4]; the side reactions can be assumed negligible under a wide range of temperature[21]. Besides, the detailed physical and thermodynamic properties of benzene and cyclohexane can be found in the literature.[22] All these make the simulation of hydrogenation of benzene to cyclohexane in Pd/γ-alumina catalyst particles feasible.

In this work, we propose a discrete model, which can describe the coupled mass transfer, reaction, and phase change in porous catalysts. Mass transfer and reaction in both liquid and vapor phases are included in this model; most importantly, the pore blocking is included by using an extended Hoshen-Kopelman algorithm[23]. We choose hydrogenation of benzene to cyclohexane over Pd/γ-alumina catalysts as the model reaction system, and validate our model by comparing with the corresponding experiments and a continuum model[4]. Lastly, the pore blocking effects on the hysteresis in effectiveness factor and the sensibility of these effects to the pore structure of catalyst particles are investigated by using the proposed discrete model.

Modeling

The proposed discrete model consists of three tightly coupled parts, namely: the pore network, mass transfer and reaction, and phase change. Pore networks are constructed to represent the pore structure of catalyst particles, as illustrated in Fig. 1; equations of mass transfer and reaction in the pore network are solved to generate the concentration profile; the phase state in each pore, which should be known before calculating the parameters characterising the equations of mass transfer and reaction, is determined by using capillary condensation and pore blocking theories. The three parts are integrated into an overall algorithm, discussed further on and shown in Fig. 3.

This article is protected by copyright. All rights reserved.

Accepted Article

In this work, hydrogenation of benzene to cyclohexane over Pd/γ-alumina catalysts is used as the model reaction system.

The particle temperature is assumed to be constant, which is reasonable even for catalysts with very high activity if the thermal conductivity of catalysts is not too low[37]. The difference between bulk temperature and particle temperature caused by the release of reaction heat is not included in this work. However, if the discrete model is to be inserted in a reactor model, these nonisothermal effects must be included.

Pore network

We build three-dimensional (cubic, within a spherical domain), and two-dimensional (square) pore networks for separate simulations and purposes, as shown in Fig. 1. The pores are assumed to be cylindrical. For an independent cylindrical pore, there is no pore blocking phenomenon; only when connecting cylindrical pores and then forming a pore network, pore blocking can happen. If there are some ink-bottle pores, the situation could be more complex, because pore blocking can even occur in an independent ink-bottle pore.

The three-dimensional pore networks in a spherical domain are used to validate the proposed discrete model, because the Pd/γ-alumina catalyst particles used in the experiments[4] for the validation are spherical; the two-dimensional square pore networks are employed to probe the pore blocking effects on multiphase reactions, because these pore networks are adequate to grasp some of the main features of the pore structure in real catalyst particles, while using these pore networks reduces the computational cost to within a reasonable limit. It is worth noting that two-dimensional pore networks are not able to describe the shape of real catalysts. If one wants to investigate the effects of shape, three-dimensional pore networks must be used. In this work, we focus on investigating the effects of connectivity and pore size distribution. Two-dimensional

This article is protected by copyright. All rights reserved.

Accepted Article

pore networks should be adequate, although quantitative but not qualitative differences in results could be expected when using three-dimensional pore networks.

As shown in Fig. 1, the pore bodies corresponding to the nodes of the network are treated as zero-volume intersections; while all the pore volume is attributed to the throats or channels[24-26]. The nodes are uniformly distributed, and the number of nodes are increased until obtaining consistent simulation results.[19,20] The pores between two adjacent nodes are allocated according to the connectivity, and radius of each pore channel is randomly assigned, following a log-normal distribution[4]:

$$f(r) = \frac{V_t}{\sqrt{2\pi} r \sigma} \exp\left[-\frac{(\ln r - \ln r_a)^2}{2\sigma^2} \right] \quad (1)$$

where *f(r)* is the pore size distribution (PSD) density at radius r, V_t is the total pore volume of the catalyst particles, r_a is the volume-averaged radius, and σ is the standard deviation. To avoid undersized or oversized pores, we limit pore radii in a reasonable range [r_{low}, r_{high}], where the values of cumulative distribution function of the log-normal distribution are between 0.001 and 0.999.

Mass transfer and reaction

Mass transfer and reaction in both vapor and liquid phases simultaneously occur in the pore network. This process is described by using different types of equations in the pore channels and the nodes. In the pore channels, a continuity equation is used to describe diffusion and reaction; in nodes, Kirchhoff's current law is satisfied due to the assumption of zero-volume nodes. It is worth noting that the parameters of diffusion and reaction in vapor-filled and liquid-filled pores are different, although the equations for these pores are essentially the same, if convective flow can be ignored. We also assume that contributions from surface diffusion are minimal and the temperature gradient in the catalyst particle is negligible.

This article is protected by copyright. All rights reserved.

Accepted Article

In the pore channels, the continuity equation, for component *i*, involving diffusion and reaction is thus given by:

$$\frac{dJ_{i,n}}{dl_n}\frac{r_n}{2} - R_i = 0 \tag{2}$$

where J_i is the diffusion flux of component *i* in pore *n,* R_i is the reaction rate per pore surface area of component *i*, l_n is the length of pore *n*, and r_n is the radius of pore *n*. Because benzene and cyclohexane are very close in physical and thermodynamic properties,[4,21] our model reaction system can be regarded as a binary mixture, i.e., benzene and cyclohexane as one component mixed with hydrogen. Fick's law is strictly valid for binary mixtures.[35] Therefore, to reduce the computational cost, Fick's law rather than the Dusty Gas model is employed:

$$J_{i,n} = -D_{i,n}\frac{dC_{i,n}}{dl_n} \tag{3}$$

where $D_{i,n}$ and $C_{i,n}$ are the effective diffusivity and the concentration of component *i* in the mixture, in pore *n*. For reacting systems consisting of more than two components with different properties, the Maxwell-Stefan equations should be used to calculate the diffusion fluxes.[26]

For vapor-filled pores, $D_{i,n}$ is calculated by using the Bosanquet equation[27]:

$$D_{i,n} = \frac{D_{i,m}D_{i,k}}{D_{i,m} + D_{i,k}} \tag{4}$$

in combination with the Wilke approximation:

$$D_{i,m} = \frac{1 - x_i}{\sum_{\substack{i=1 \\ j \neq i}}^{n} \frac{x_j}{D_{i,j}}} \tag{5}$$

where $D_{i,k}$ is the Knudsen diffusivity of component *i*, $D_{i,m}$ is the molecular diffusivity of component *i*, $D_{i,j}$ is the binary diffusivity of component *i* in mixture of *i* and *n* components *j*, and x_i is the mole fraction of component *i*. Fick's law with the Bosanquet equation as Fickian

This article is protected by copyright. All rights reserved.

diffusivity is a very good approximation for the Dusty Gas model, even when temperature (~800 K) and pressure (~80 bar) are very high.[27] For liquid-filled pores, $D_{i,n}$ is calculated by employing the Tyn and Calus method[28]:

$$D_{i,n} = 8.93\times10^{-12}\frac{V_B^{0.267}}{V_i^{0.433}}\frac{T}{\mu_B}\left(\frac{\delta_B}{\delta_i}\right)^{0.15} \tag{6}$$

where: V_i is the molar volume of component i at its normal boiling temperature; V_B, the molar volume of benzene at its normal boiling temperature, is regarded as the molar volume of the solvent at its normal boiling temperature; μ_B is the dynamic viscosity of benzene; T is the temperature; δ_B and δ_i are surface tensions for the component i and benzene. An expression for the reaction rate per pore surface area of component i for vapor-filled pores ($R_{i,v}$) and liquid-filled pores ($R_{i,l}$) can be found elsewhere[4], and is presented in Eq. (7) and Eq. (8), respectively:

$$R_{i,v} = \frac{0.199 v_i \exp\left(\frac{-28250}{RT}\right)\frac{P_B}{10}\left(\frac{P_H}{10}\right)^{0.5}\frac{1}{S}}{\left[1+1.80\times10^{-4}\exp\left(\frac{41170}{RT}\right)\frac{P_B}{10}\right]\left[1+2.95\times10^{-2}\exp\left(\frac{-9370}{RT}\right)\left(\frac{P_H}{10}\right)^{0.5}\right]} \tag{7}$$

$$R_{i,l} = 0.436 v_i \exp\left(\frac{-43880}{RT}\right)\frac{P_H}{10}\frac{1}{S} \tag{8}$$

where v_i is the stoichiometric number of component i, P_B is the partial pressure of benzene, P_H is the partial pressure of benzene, R is the universal gas constant, and S, the surface area of the catalyst Pd/γ-alumina, is 246.6m^2/g.[4]

In the inner nodes, Kirchhoff's current law is employed:

$$\sum_{n=1}^{n=Z}\pi r_n^2 J_{i,n} = 0 \tag{9}$$

where Z is the connectivity; as to the boundary nodes, Robin boundary conditions are given as follows

This article is protected by copyright. All rights reserved.

Accepted Article

$$-k_i(C_{i,b} - C_{i,n}) = -D_{i,n}\frac{dC_{i,n}}{dl_n} \tag{10}$$

where k_i is the mass transfer coefficient of component i in the catalyst surface film, and $C_{i,b}$ is the bulk concentration of component i.

Phase change

For independent pores, i.e., the pores without connections to other pores, capillary condensation theory alone is adequate to determine the phase state in these pores if the conditions (e.g., concentration of each component and temperature) in these pores are known. In our case, pore blocking theory, however, must be included, because the phase state of connected pores can be significantly affected by pore blocking. As mentioned before, the liquid mixture can be regarded as pure benzene when determining the phase state, because benzene and cyclohexane are very close in physical properties.

At any given condition, by comparing the critical pore radius of capillary condensation (r_c) with the real pore radius, one can determine the phase state in a particular pore. During condensation, a pore is vapor-filled when its radius is larger than r_c. During evaporation, not all pores with radius larger than r_c are filled with vapor, because of the pore blocking effect. The liquid in some large pores, e.g., ink-bottle pores, can be trapped by the liquid in their adjacent pores. These large pores stay filled with liquid until the liquid in at least one of their adjacent pores has evaporated, as shown in Fig. 2. In this work, the extended Hoshen-Kopelman algorithm[23] is employed to identify these pores with blocked liquid. The extended Hoshen-Kopelman algorithm is able to handle any pore network, regardless of whether the pore network is two-dimensional or three-dimensional, uniform or random, cubic or in any other topology.

The critical pore radius of capillary condensation (r_c) is

$$r_c = t + r_k \tag{11}$$

This article is protected by copyright. All rights reserved.

Accepted Article

where t is the layer thickness, and r_k is the Kelvin radius. The layer thickness (t) is obtained from a modified Halsey equation[29]:

$$t = t_m \left[\frac{5}{\ln\left(P_s / P\right)} \right]^{1/3} \left(\frac{P}{P_s} \right)^m \tag{12}$$

where t_m is the monolayer molecular thickness, P_s is the saturation vapor pressure of the adsorbate, P is the pressure of the adsorbate, and m is an unknown parameter that needs to be determined by experiments. Cheng et al.[22] reported that m for benzene is 0.4, and t_m for benzene is

$$t_m = 0.1 + 7.57 \times 10^{-4} T \tag{13}$$

The Kelvin radius (r_k) is determined by using the Kelvin equation for evaporation (Eq. (14)) and Cohan equation for condensation (Eq. (15)), because the meniscus shape is close to hemispherical during evaporation and cylindrical during condensation, respectively.

$$\mathrm{r}_k = \frac{2M\delta}{RT\rho \ln\left(\frac{P_s}{P}\right)} \tag{14}$$

$$\mathrm{r}_k = \frac{M\delta}{RT\rho \ln\left(\frac{P_s}{P}\right)} \tag{15}$$

In these equations, M is the average molecular weight of the adsorbate, δ is the surface tension of the adsorbate, and ρ is the density of the adsorbate. However, in some reaction systems with non-ideal mixtures, e.g., hydrodesulphurization reactions[19,20], a multicomponent version of the Kelvin equation[30] should be employed to determine r_k. Also, these equation should be replaced by more

This article is protected by copyright. All rights reserved.

accurate ones for narrow mesopores, e.g., based on nonlocal density functional theory (NLDFT)[31,36].

Implementation

The overall algorithm is presented in Fig. 3, and implemented in Matlab. In step 1, the pore network is constructed according to the assigned topological and geometrical parameters, and then the initial guess of concentration and phase state is allocated to each pore. Step 2 aims to get the concentrations in all pore channels by simulating mass transfer and reaction in the pore network. The function 'fsolve' in Matlab is used to simultaneously and iteratively solve Eq. (2), Eq. (9), and Eq. (10) for all pore channels and nodes. This iteration process does not stop until the simulation has converged. During this process, the phase states calculated from step 3, and the parameters for diffusion and reaction in the vapor and liquid phases are constantly fed into the simulation. After getting these concentrations, step 3 is performed to determine the phase state for each pore channel. If the new phase states are different from the previous ones, the process goes back to step 2; if unchanged phase states in all the pore channels are obtained, the results are output and the process stops.

After obtaining the concentrations and phase states in all the pore channels, the effectiveness factor (η) of the catalyst particle is calculated by

$$\eta = \frac{\sum_{n=1}^{N} 2\pi r_n l_n R_C\left(C_{B,n}, C_{H,n}, T\right)}{\sum_{n=1}^{N} 2\pi r_n l_n R_C\left(C_{B,b}, C_{H,b}, T\right)} \tag{16}$$

where N is total number of pores. Then, the effectiveness factors of catalyst particles with different pore structures and under different bulk pressures of benzene and temperatures are calculated to investigate how pore blocking affects the multiphase reactions and how pore

This article is protected by copyright. All rights reserved.

structure changes the pore blocking effects. In addition, the wetting fraction (f_w) in the catalyst particles is calculated by

$$f_w = \frac{V - V_s}{V_t - V_s} = \frac{\sum_{n=1}^{N_l} \pi r_n^2 l_n}{\sum_{n=1}^{N} \pi r_n^2 l_n - \sum_{n=1}^{N_v} 2\pi r_n l_n t_n} \tag{17}$$

where V is the total adsorbed volume, V_t is the total pore volume of the catalyst, V_s is the saturated multilayer adsorption volume, and N_l and N_v are the number of liquid-filled pores and vapor-filled pores, respectively[22]. The pore blocking effects on the wetting fraction are also investigated to support the explanations of the pore blocking effects on multiphase reactions, which is shown in the supporting information.

Results and Discussion

Model validation

The proposed discrete model is validated by comparing with a continuum model and experiments at the particle level[4]. Parameters for this model validation are presented in Table 1, and results are shown in Fig. 4. The number of nodes, i.e., 5649, is adequate and reasonable, because the simulation results are almost the same but computational cost increases significantly when adding more nodes; the gas-solid mass transfer coefficients, which are fitted from the experiments, are within the reasonable range reported in the literature[32,33]; the other parameters are obtained from elsewhere[4,34].

When plotting the effectiveness factor of the catalyst particle as a function of the bulk pressure of benzene, a hysteresis loop is formed, as shown in Fig. 4. The condensation branch of the steady states is well above the evaporation branch. The internal wetting fraction of the catalysts during condensation (increasing bulk pressure of benzene) is much lower than the one during evaporation (decreasing bulk pressure of benzene), which can be found in the supporting

This article is protected by copyright. All rights reserved.

Accepted Article

information. The inconsistent wetting fractions would lead to different effectiveness factors (η), because the reaction rate in the vapor phase is different from the one in the liquid phase according to Eq. (7) and (8). More detailed explanations are included in the supporting information. Therefore, there are two steady states at the same reaction condition.

The effectiveness factors calculated by the discrete model are much closer to the experimental ones when comparing with the ones predicted by the continuum model, and, therefore, the discrete model is more accurate than the continuum model. The proposed discrete model includes pore blocking, but the continuum model did not do this, which is likely to be the main reason why the discrete model is better. Zhou et al.[4] assumed that the film resistance on the surface of catalyst particles is negligible in their continuum model, but we include the film resistance in the proposed discrete model (see Eq. (10)), which could be another reason.

Meanwhile, Fig. 5 is given to provide direct insight into which fraction of the reaction rate occurs in the vapor-filled and liquid-filled pores. There are two branches of reaction rates (see the solid lines in Fig. 5), due to reaction rate hysteresis. The reaction rates of vapor-filled pores decrease with the bulk pressure of benzene, because of the decrease in the number of vapor-filled pores; the ones of liquid-filled pores increase with the bulk pressure of benzene, because of the increase in the number of liquid-filled pores. The condensation branch of the reaction rate in the vapor-filled pores is well above the corresponding evaporation branch, because more pores are filled with vapor during condensation; the evaporation branch of the reaction rate in the liquid-filled pores is well above the corresponding condensation branch, because more pores are filled with liquid during evaporation.

Pore blocking effects on hysteresis in effectiveness factors

In this section, pore blocking effects on the multiphase reaction, which are reflected by how pore blocking changes the hysteresis in effectiveness factors, are probed using a 2D model; the

This article is protected by copyright. All rights reserved.

relationships between pore network parameters, i.e., connectivity and pore size distribution, and pore blocking effects are investigated. The parameters used to simulate pore blocking effects are presented in Table 2. The number of nodes is set at 1681 (41×41), because increasing the nodes only causes negligible differences in the simulation results but the computational cost would increase significantly. The film resistance of the catalyst outer surface is assumed to be negligible when probing pore blocking effects, i.e., the mass transfer coefficient of component i (k_i in Eq. (10)) is assumed to be infinitely large for practical purposes. This assumption is made, because the mass transfer coefficient would not qualitatively affect the results in this section and the mass transfer coefficient can be very difficult to predict accurately with changing reaction conditions. Therefore, Dirichlet boundary conditions are assumed in this section:

$$C_{i,n} = C_{i,b} \tag{18}$$

To quantify the pore blocking effects on the hysteresis in effectiveness factor, a parameter f_{PB} is introduced, which defines the proportion of the hysteresis loop area that can be associated to pore blocking effects:

$$f_{PB} = \frac{S_{PB}}{S_t} \tag{19}$$

where S_{PB} is the hysteresis loop area caused by pore blocking effects and S_t is the total hysteresis loop area. When including the extended Hoshen-Kopelman algorithm[23] in our discrete model to describe pore blocking, one obtains the evaporation branch of the effectiveness factor with pore blocking effects included (see red dashed line in Fig. 6); when removing this algorithm from our model, one obtains the evaporation branch with pore blocking effects excluded (see blue dotted line in Fig. 6). The area between the two evaporation branches is the hysteresis loop area caused by pore blocking effects, which reflects the importance level of pore blocking in affecting the hysteresis in effectiveness factors.

This article is protected by copyright. All rights reserved.

Accepted Article

Accepted Article

Fig. 6a indicates that 42% of the hysteresis loop area is caused by pore blocking when the effectiveness factors are presented as a function of bulk pressure of benzene changing from 3 bar to 7 bar; Fig. 6b shows that 44% of the hysteresis loop area is caused by pore blocking when the effectiveness factors are plotted against a change in particle temperature from 415 K to 460 K. These results indicate that pore blocking significantly affects multiphase reactions and must be included when simulating multiphase reactions in porous catalyst particles. Then, it becomes interesting to probe the sensitivities of the pore blocking effects to the pore structure of catalyst particles, e.g., connectivity and pore size distribution. These results are shown in Fig. 7, Fig. 8, and Fig. 9.

Fig. 7 shows the percentage of the hysteresis loop area caused by pore blocking (f_{PB}) as a function of connectivity (Z). The f_{PB} decreases significantly when increasing connectivity from 3 to 6, changing from 42% to 18%, when varying benzene pressure as illustrated in Fig.7a, and from 44% to 17%, when varying temperature as shown in Fig. 7b. These results indicate that pore blocking effects on the hysteresis in effectiveness factors can be significantly weakened when the connectivity of the pore network is sufficiently high. By changing the wetting fraction in a catalyst particle, pore blocking affects the hysteresis in effectiveness factor, which is shown in the supporting information. The blocked liquid in pores that have more adjacent pores connected to them evaporates more easily during a reduction in pressure or an increase in temperature, because trapped liquid in a pore can be released if liquid in one of their adjacent pores has evaporated. Therefore, a well-connected pore network largely reduces the difference in wetting fractions between evaporation and condensation, and then significantly weakens pore blocking effects.

Fig. 8 and Fig. 9 show the sensitivity of pore blocking effects to pore size distribution (PSD), which is described by Eq. (1). Fig. 8 presents the proportion of the hysteresis loop area caused by pore blocking as a function of the standard deviation. Pore blocking effects are very sensitive to

This article is protected by copyright. All rights reserved.

Accepted Article

the standard deviation, with f_{PB} increasing from 0% to 46%, as shown in Fig. 8a (change in P_B), and from 0% to 47%, as shown in Fig. 8b (change in T), when changing the standard deviation from 0 to 0.7. These results show that pore blocking effects can be significantly enhanced when the standard deviation of the PSD is large. A large standard deviation indicates a wide distribution of pore size according to Eq. (1), and also means that broad pores are more likely to be surrounded by narrow pores; in this case, liquid in broad pores is more easily trapped by liquid in adjacent pores, because liquid in narrow pores does not easily evaporate. Therefore, a wide pore size distribution largely increases the difference in wetting fractions between evaporation and condensation, and then significantly enhances pore blocking effects.

Fig. 9 shows the proportion of the hysteresis loop area caused by pore blocking as a function of the volume-averaged pore radius of the PSD described in Eq. (1). The fluctuation of f_{PB} is not significant when changing the volume-averaged pore radius from 2.5 nm to 20 nm, fluctuating between 23% and 31%, as shown in Fig. 9a (change in P_B), and between 25% and 33%, as illustrated in Fig. 9b (change in T). These results indicate that the volume-averaged pore radius can only slightly change pore blocking effects. A change in volume-averaged pore radius would not change the shape of PSD curve, which indicates that the ratio between the radii of the narrow pores and broad pores would not change significantly. Therefore, the volume-averaged pore radius would not significantly change pore blocking effects within the range of mesopore size (1-25 nm, according to IUPAC). It is worth noting that f_{PB} cannot be accurately calculated when the volume-averaged pore radius is above 25 nm, because the hysteresis loop area can be very small. Also, for very narrow pores, the effect of surface diffusion could become more significant.

During multiphase reactions in catalysts, the pore network structure, including connectivity and pore size distribution, can be considered as unchanged, because the liquid-filled pores can also contribute to mass transfer and reaction rate, just as vapour-filled pores. However, for

This article is protected by copyright. All rights reserved.

deactivation caused by coking in catalysts, the blocked pores filled with coke cannot contribute to mass transfer and reaction rate, and the pore network structure would change with time. Thus, the pore network parameters discussed in this work are applied for all pores, whether they are open or (partially) blocked.

Conclusions

A discrete pore network model was used to simulate multiphase reactions in porous catalyst particles. This model was validated by comparing results with those from a continuum model and experiments reported before[4], for the hydrogenation of benzene to cyclohexane in Pd/γ-alumina catalyst particles. For the first time, pore blocking effects on the hysteresis in effectiveness factor were evaluated, and their relationship with catalyst pore network structure was probed.

The simulation results show that pore blocking effects contribute to up to 50% of the hysteresis loop area in some cases, indicating that pore blocking effects on multiphase reactions in catalyst particles are very important and must be considered when modeling such reactions. Pore blocking effects are significantly enhanced when decreasing the pore network connectivity (changing it from 6 to 3) or increasing the standard deviation of the PSD described in Eq. (1) (changing it from 0 to 0.7); the volume-averaged pore radius of the PSD (changing it between 2.5 nm and 20 nm), however, is not important in inducing pore blocking effects.

These insights are useful when modeling and designing multiphase catalytic processes, and should be considered in reactor models. They are also relevant to assist the design of porous catalytic materials, in order to achieve a particular hysteretic behavior or a desired catalytic state. The discrete model in this work can be adapted to represent structural heterogeneities, e.g., bidisperse pore networks or core-shell particles, which are more representative of real catalyst pellets than random pore networks. Moreover, the discrete model may also be adapted to simulate liquid imbibition; when some fluid contacts catalysts particles, this phenomenon could

This article is protected by copyright. All rights reserved.

Accepted Article

become significant[13]. These will become our future work.

AUTHOR INFORMATION

First Corresponding Author

*Tel.: +86-21-64253509. Fax: +86-21-64253528. E-mail: xgzhou@ecust.edu.cn

Second Corresponding Author

†Tel.: +44-20-31081126. Fax.: +44-20-73832348. Email address: m.coppens@ucl.ac.uk

Acknowledgments

The authors are grateful for the financial support of the National Basic Research Program of China (2012CB720501) and the National Natural Science Foundation of China (U1162112 and 21376076), as well as support from the UK's EPSRC "Frontier Engineering" Centre for Nature Inspired Engineering (EP/K038656/1). G. Y. is supported by the China Scholarship Council (CSC) for his research at UCL.

Notation

$C_{i,n}$ concentration of component *i* in pore *n*, mol/m^3

$C_{i,b}$ bulk concentration of component *i*, mol/m^3

d diameter of the catalyst particle, mm

$D_{i,j}$ binary diffusivity of component *i* in mixture of *i* and *j*, m^2/s

$D_{i,k}$ Knudsen diffusivity of component i, m^2/s

$D_{i,m}$ molecular diffusivity of component i, m^2/s

$D_{i,n}$ effective diffusivity of component *i* in pore *n*, m^2/s

f_{PB} proportion of hysteresis loop area caused by pore blocking effect, dimensionless

This article is protected by copyright. All rights reserved.

f_w wetting fraction, dimensionless

$f(r)$ pore size distribution density at radius r, $cm^3/g/nm$

$J_{i,n}$ diffusion flux of component i in pore n, $mol/m^2/s$

k_i mass transfer coefficient of component i, m/s

$k_{B,gs}$ gas-solid mass transfer coefficient for benzene, m/s

$k_{C,gs}$ gas-solid mass transfer coefficient for cyclohexane, m/s

$k_{H,gs}$ gas-solid mass transfer coefficient for hydrogen, m/s

L side length of the model catalyst, mm

l_n length of pore n, m

M molecular weight, g/mol

N_l number of liquid-filled pores, dimensionless

N_v number of vapor-filled pores, dimensionless

P pressure, bar

P_B partial pressure of benzene, bar

$P_{B,b}$ bulk pressure of benzene, bar

$P_{C,b}$ bulk pressure of cyclohexane, bar

P_H partial pressure of hydrogen, bar

P_s saturation vapor pressure of the adsorbate, bar

P_t total pressure, bar

r pore radius, nm

r_a volume-averaged pore radius, nm

r_c critical pore radius of capillary condensation, nm

r_k Kelvin radius, nm

r_n radius of pore n, m

This article is protected by copyright. All rights reserved.

R universal gas constant, J/mol/K

R_i reaction rate per pore surface area of component i, mol/m^2/s

R_C reaction rate per pore surface area of cyclohexane, mol/m^2/s

$R_{i,v}$ reaction rate per pore surface area of component i for vapor-filled pores, mol/m^2/s

$R_{i,l}$ reaction rate per pore surface area of component i for liquid-filled pores, mol/m^2/s

$R_{C,v}$ reaction rate per pore surface area of cyclohexane for vapor-filled pores, mol/m^2/s

$R_{C,l}$ reaction rate per pore surface area of cyclohexane for liquid-filled pores, mol/m^2/s

S surface area of the catalyst, m^2/g

S_t total hysteresis loop area, dimensionless

S_{PB} hysteresis loop area caused by pore blocking effect, dimensionless

t layer thickness, nm

t_m monolayer molecular thickness, nm

t_n adsorbed layer thickness in pore n, m

T temperature, K

v_i stoichiometric number of component i, dimensionless

V total adsorbed volume in the model catalyst, m^3

V_s saturated multilayer adsorption volume in the model catalyst, m^3

V_t total pore volume of the model catalyst, m^3

V_B molar volume of benzene at its normal boiling point, m^3/mol

V_i molar volume of component i at its normal boiling point, m^3/mol

x_i mole fraction of component i, dimensionless

Z pore network connectivity, dimensionless

Greek Letters

σ standard deviation, dimensionless

This article is protected by copyright. All rights reserved.

Accepted Article

μ viscosity, cP

δ surface tension, N/m

ρ density, kg/m^3

η effectiveness factor, dimensionless

Subscripts and Superscripts

a average

B benzene

b bulk

C cyclohexane

c critical

gs gas-solid film

H hydrogen

i, j,n species type

l liquid phase

PB pore blocking

s saturation

t total

v vapor phase

w wetting

Accepted Article

This article is protected by copyright. All rights reserved.

Accepted Article

References

1. Hessari FA, Bhatia SK. Reaction rate hysteresis in a single partially internally wetted catalyst pellet: experiment and modelling. *Chem. Eng. Sci.* 1996;51:1241-1256.
2. Kim DH, Kim YG. An experimental study of multiple steady states in a porous catalyst due to phase transition. *J. Chem. Eng. Japan.* 1981;14:311-317.
3. Watson PC, Harold MP. Rate enhancement and multiplicity in a partially wetted and filled pellet: experimental study. *AIChE J.* 1994;40:97-111.
4. Zhou Z-M, Cheng Z-M, Li Z, Yuan W-K. Determination of effectiveness factor of a partial internal wetting catalyst from adsorption measurement. *Chem. Eng. Sci.* 2004;59:4305-4311.
5. Jaguste DN, Bhatia SK. Partial internal wetting of catalyst particles: hysteresis effects. *AIChE J.* 1991;37:650-660.
6. Cohan LH. Hysteresis and the capillary theory of adsorption of vapors. *JACS*. 1944;66:98-105.
7. Horikawa T, Do DD, Nicholson D. Capillary condensation of adsorbates in porous materials. *Adv. Colloid Interface Sci.* 2011;169:40-58.
8. Lilly MP, Finley PT, Hallock RB. Memory, congruence, and avalanche events in hysteretic capillary condensation. *Phys. Rev. Lett.* 7 1993;1:4186-4189.

This article is protected by copyright. All rights reserved.

Accepted Article

9. Mason G. Determination of the pore-size distribution and pore-space interconnectivity of vycor porous glass from adsorption-desorption hysteresis capillary condensation isotherms. *Proc. R. Soc. Lond. A.* 1988;415:453-486.

10. Rajniak P, Yang RT. A simple model and experiments for adsorption-desorption hysteresis: water vapor on silica gel. *AIChE J.* 1993;39:774-786.

11. Rajniak P, Yang RT. Hysteresis-dependent adsorption-desorption cycles: generalization for isothermal conditions. *AIChE J.* 1994;40:913-924.

12. Seaton NA. Determination of the connectivity of porous solids from nitrogen sorption measurements. *Chem. Eng. Sci.* 1991;46:1895-1909.

13. Mikhailova IA, Kirillov VA, Fadeev SI, Slinko MG. Mathematical modelling of exothermic catalytic reaction in a single partially-wetted porous catalyst particle. *Chem. Eng. J.* 2003;91:181-189.

14. Sakornwimon W, Sylvester ND. Effectiveness factors for partially wetted catalysts in trickle-bed reactors. *Ind. Eng. Chem. Process Des. Dev.* 1982;21:16-25.

15. Sahimi M, Gavalas GR, Tsotsis TT. Statistical and continuum models of fluid-solid reactions in porous media. *Chem. Eng. Sci.* 1990;45:1443-1502.

16. Keil FJ. Diffusion and reaction in porous networks. *Catal. Today.* 1999;53:245-258.

17. Coppens M.-O, Froment GF. Diffusion and reaction in a fractal catalyst pore-I. geometrical aspects. *Chem. Eng. Sci.* 1995;50:1013-1026.

This article is protected by copyright. All rights reserved.

Accepted Article

18. Coppens M.-O. The effect of fractal surface roughness on diffusion and reaction in porous catalysts - from fundamentals to industrial applications. *Catal. Today*. 1999;53:223-242.

19. Wood J, Gladden LF, Keil FJ. Modeling diffusion and reaction accompanied by capillary condensation using three-dimensional pore networks. part 2. dusty gas model and general reaction kinetics. *Chem. Eng. Sci.* 2002;57:3047-3059.

20. Wood J, Gladden LF. Modeling diffusion and reaction accompanied by capillary condensation using three-dimensional pore networks. part 1. fickian diffusion and pseudo-first-order reaction kinetics. *Chem. Eng. Sci.* 2002;57:3033-3045.

21. Cheng Z-M, Anter AM, Yuan W-K. Intensification of phase transition on multiphase reactions. *AIChE J.* 2001;47:1185-1192.

22. Cheng Z-M, Zhou Z-M, Yuan W-K. Determination of catalyst wetting fraction on the molecular level. *AIChE J.* 2007;53:741-745.

23. Al-Futaisi A, Patzek TW. Extension of Hoshen-Kopelman algorithm to non-lattice environments. *Physica A*. 2003;321:665-678.

24. Sharratt PN, Mann R. Some observations on the variation of tortuosity with Thiele modulus and pore size distribution. *Chem. Eng. Sci.* 1987;42:1565-1576.

25. Hollewand MP, Gladden LF. Modelling of diffusion and reaction in porous catalysts using a random three-dimensional network model. *Chem. Eng. Sci.* 1992;47:1761-1770.

26. Rieckmann C, Keil FJ. Multicomponent diffusion and reaction in three-dimensional networks: general kinetics. *Ind. Eng. Chem. Res.* 1997;36:3275-3281.

This article is protected by copyright. All rights reserved.

Accepted Article

27. Solsvik S, Jakobsen HA. Modeling of multicomponent mass diffusion in porous spherical pellets: application to steam methane reforming and methanol synthesis. *Chem. Eng. Sci.* 2011;66:1986-2000.

28. Poling BE, Prausnitz JM, O' Connell JP. The properties of gases and liquids (5th edition). Boston:McGraw-Hill, 2001.

29. Androutsopoulos GP, Salmas CE. A new model for capillary condensation-evaporation hysteresis based on a random corrugated pore structure concept: prediction of intrinsic pore size distribution. 2. model application. *Ind. Eng. Chem. Res.* 2000;39:3764–3777.

30. Shapiro AA, Stendy EH. Kelvin equation for a non-ideal multicomponent mixture. *Fluid Phase Equilibrium.* 1997;134:87-101.

31. Thommes M, Smarsly B, Groenewolt M, Ravikovitch PI, Neimark AV. Adsorption hysteresis of nitrogen and argon in pore networks and characterization of novel micro- and mesoporous silicas. *Langmuir*. 2006;22:756-764.

32. Al-Dahhan MH, Larachi F, Dudukovic MP, Laurent A. High-pressure trickle-bed reactors: a review. *Ind. Eng. Chem. Res.* 1997;36:3292-3314.

33. Losey MW, Schmidt MA, Jensen KF. Microfabricated multiphase packed-bed reactors: characterization of mass transfer and reactions. *Ind. Eng. Chem. Res*. 2001;40:2555-2562.

34. Murray KL, Seaton NA, Day MA. An adsorption-based method for the characterization of pore networks containing both mesopores and macropores. *Langmuir*. 1999;15:6728-6737.

35. Krishna R, Wesselingh JA. The Maxwell-Stefan approach to mass transfer. *Chem. Eng. Sci.* 1997;52:861-911.

This article is protected by copyright. All rights reserved.

Accepted Article

36. Landers J, Yu.Gor G, Neimark AV. Density functional theory methods for characterization of porous materials. *Colloids and Surfaces A: Physicochem. Eng. Aspects.* 2013;437:3-32.

37. Kehoe JPG, Butt JB. Interactions of inter- and intraphase gradients in a diffusion limited catalytic reaction. *AIChE J.* 1972;18:347-355.

This article is protected by copyright. All rights reserved.

Accepted Article

List of Table Captions

Table 1. Parameters for the model validation

Table 2. Parameters for the simulations of pore blocking effects on the multiphase reaction

This article is protected by copyright. All rights reserved.

Table 1. Parameters for the model validation

Node number	5649
Connectivity (Z)	5[b]
Diameter of the catalyst particle (d)	4 mm[a]
Total pore volume of the catalyst (V_t)	0.47 cm^3/g[a]
Volume-averaged pore radius(r_a)	3.5 nm[a]
Standard deviation (σ)	0.38[a]
Particle temperature (T)	433 K[a]
Bulk pressure of benzene ($P_{B,b}$)	4-7 bar[a]
Bulk pressure of cyclohexane ($P_{C,b}$)	≈0 bar[a]
Total pressure (P_t)	10 bar[a]
Gas-solid mass transfer coefficient for benzene ($k_{B,gs}$)	6.5×10^{-5} m/s[c]
Gas-solid mass transfer coefficient for cyclohexane ($k_{C,gs}$)	6.5×10^{-5} m/s[c]
Gas-solid mass transfer coefficient for hydrogen ($k_{H,gs}$)	4.1×10^{-4}m/s[c]

[a]Data taken from Zhou et al.[4]

[b]Data taken from Murray et al.[34]

[c]Fitted data

Accepted Article

This article is protected by copyright. All rights reserved.

Table 2. Parameters for the simulations of pore blocking effects on the multiphase reaction

Number of nodes	1681 (41×41)
Network dimensions (square $L \times L$)	4×4 mm
Connectivity (Z)	3-6
Total pore volume of the catalyst (V_t)	0.47 cm^3/g
Volume-averaged pore radius (r_a)	2.5-20 nm
Standard deviation (σ)	0-0.7
Particle temperature (T)	410-460 K
Bulk pressure of benzene ($P_{B,b}$)	3-8 bar
Bulk pressure of cyclohexane ($P_{C,b}$)	≈0 bar
Total pressure (P_t)	10 bar

Accepted Article

This article is protected by copyright. All rights reserved.

Accepted Article

List of Figure Captions

Figure 1. (a) Illustration of three-dimensional pore networks (connectivity=6); (b) illustration of two-dimensional square pore networks (connectivity=4).

Figure 2. Illustration of the pore blocking phenomenon in the pore network during the evaporation process.

Figure 3. The overall algorithm for the proposed discrete model simulating coupled diffusion, reaction and phase change in porous catalyst particles.

Figure 4. Comparison between the effectiveness factors predicted by the proposed discrete model, the continuum model[4], and experiments[4]. The arrows indicate the direction of changing the bulk pressure of benzene.

Figure 5. Reaction rates of all pores, vapor-filled pores and liquid-filled pores, as functions of bulk pressure of benzene. The parameters for simulations are presented in Table 1.

Figure 6. Illustrations of the percentage of the hysteresis loop area caused by pore blocking effects: The effectiveness factor as a function of (a) bulk pressure of benzene and (b) particle temperature. The arrows indicate the direction of a change in bulk pressure of benzene or a change in particle temperature. Fixed parameters: (a) T=433 K, Z=3, r_a=3.5 nm, and σ=0.38; (b) $P_{B,b}$=5 bar, Z=3, r_a=3.5 nm, and σ=0.38.

This article is protected by copyright. All rights reserved.

Figure 7. The proportion of the hysteresis loop area caused by pore blocking (f_{PB}) as a function of connectivity (Z). Fixed parameters: (a) T=433 K, r_a=3.5 nm, and σ=0.38; (b) $P_{B,b}$=5 bar, r_a=3.5 nm, and σ=0.38.

Figure 8. The proportion of the hysteresis loop area caused by pore blocking (f_{PB}) as a function of the standard deviation (σ) of the PSD described by Eq. (1). Fixed parameters: (a) T=433 K, Z=4, and r_a=3.5 nm; (b) $P_{B,b}$=5 bar, Z=4, and r_a=3.5 nm.

Figure 9. The proportion of the hysteresis loop area caused by pore blocking (f_{PB}) as a function of the volume-averaged pore radius (r_a) of the PSD described by Eq. (1). Fixed parameters: (a) T=433 K, Z=4, and σ=0.38; (b) $P_{B,b}$=5 bar, Z=4, and σ=0.38.

Accepted Article

This article is protected by copyright. All rights reserved.

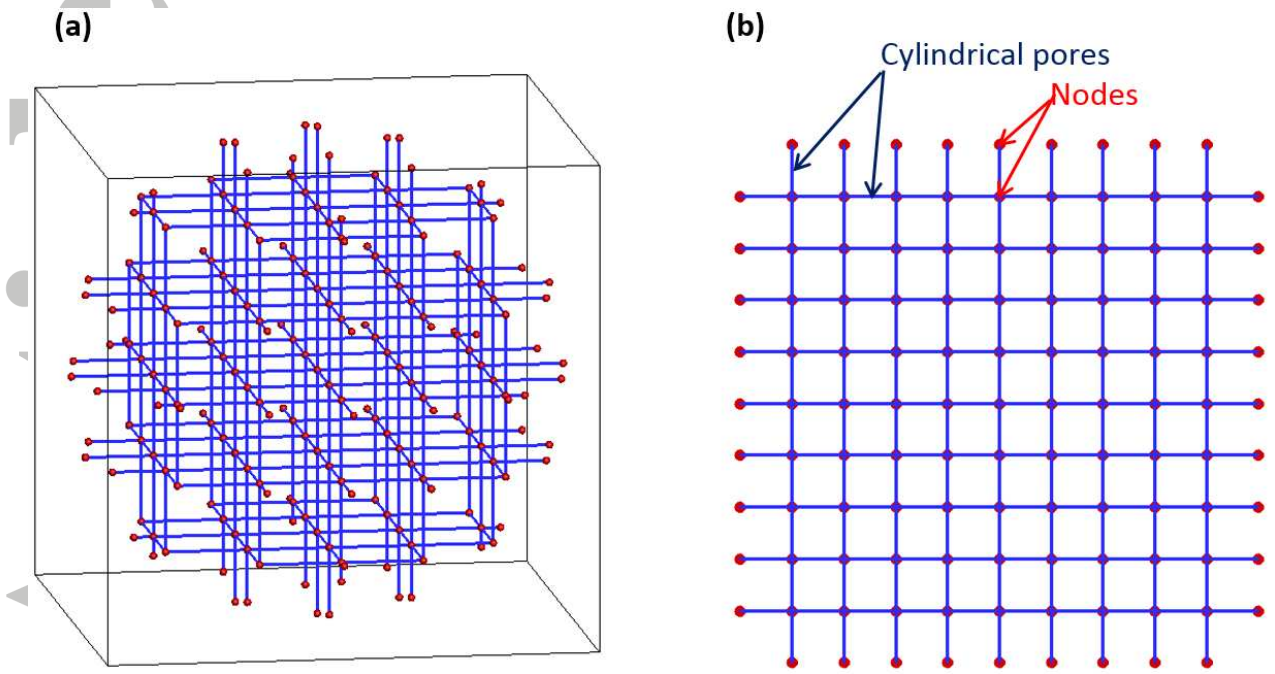

Figure 1. (a) Illustration of three-dimensional pore networks (connectivity=6); (b) illustration of two-dimensional square pore networks (connectivity=4).

Accepted

This article is protected by copyright. All rights reserved.

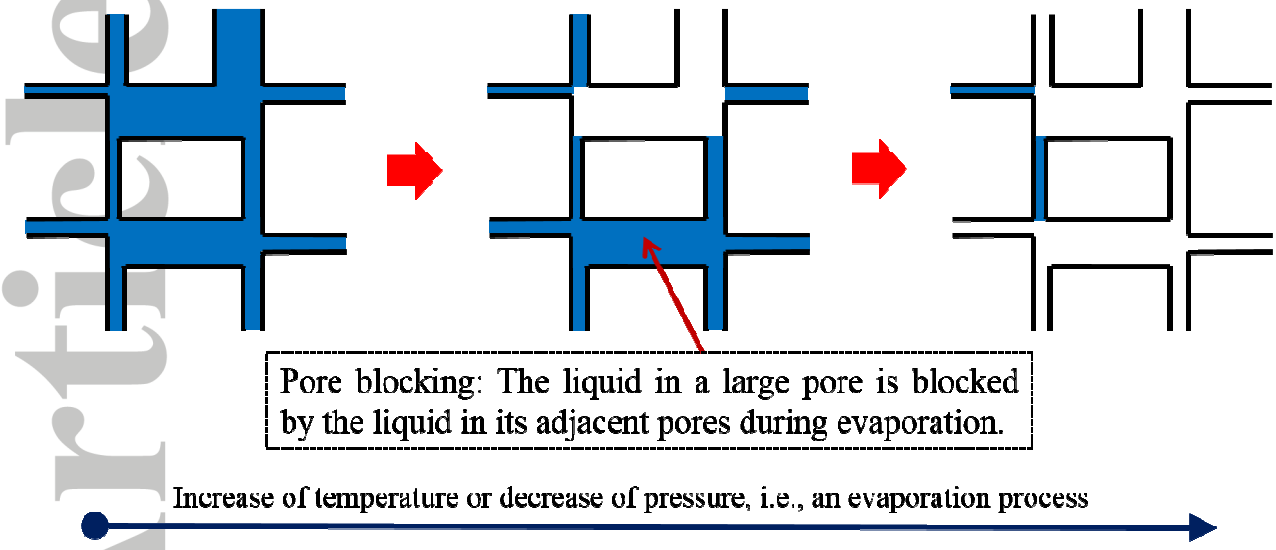

Figure 2. Illustration of the pore blocking phenomenon in the pore network during the evaporation process.

Accepted Article

This article is protected by copyright. All rights reserved.

Accepted Article

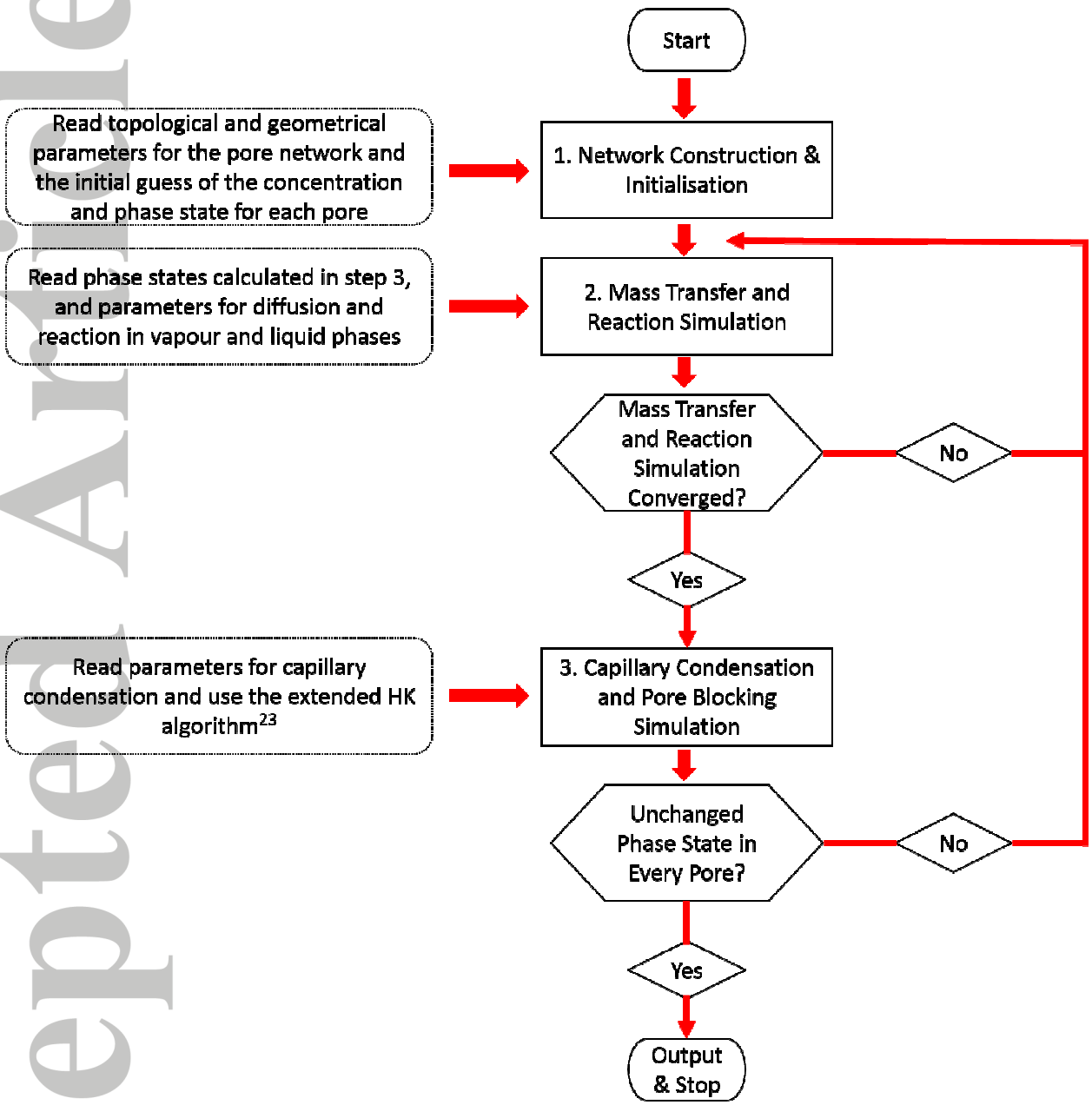

Figure 3. The overall algorithm for the proposed discrete model simulating coupled diffusion, reaction and phase change in porous catalyst particles.

This article is protected by copyright. All rights reserved.

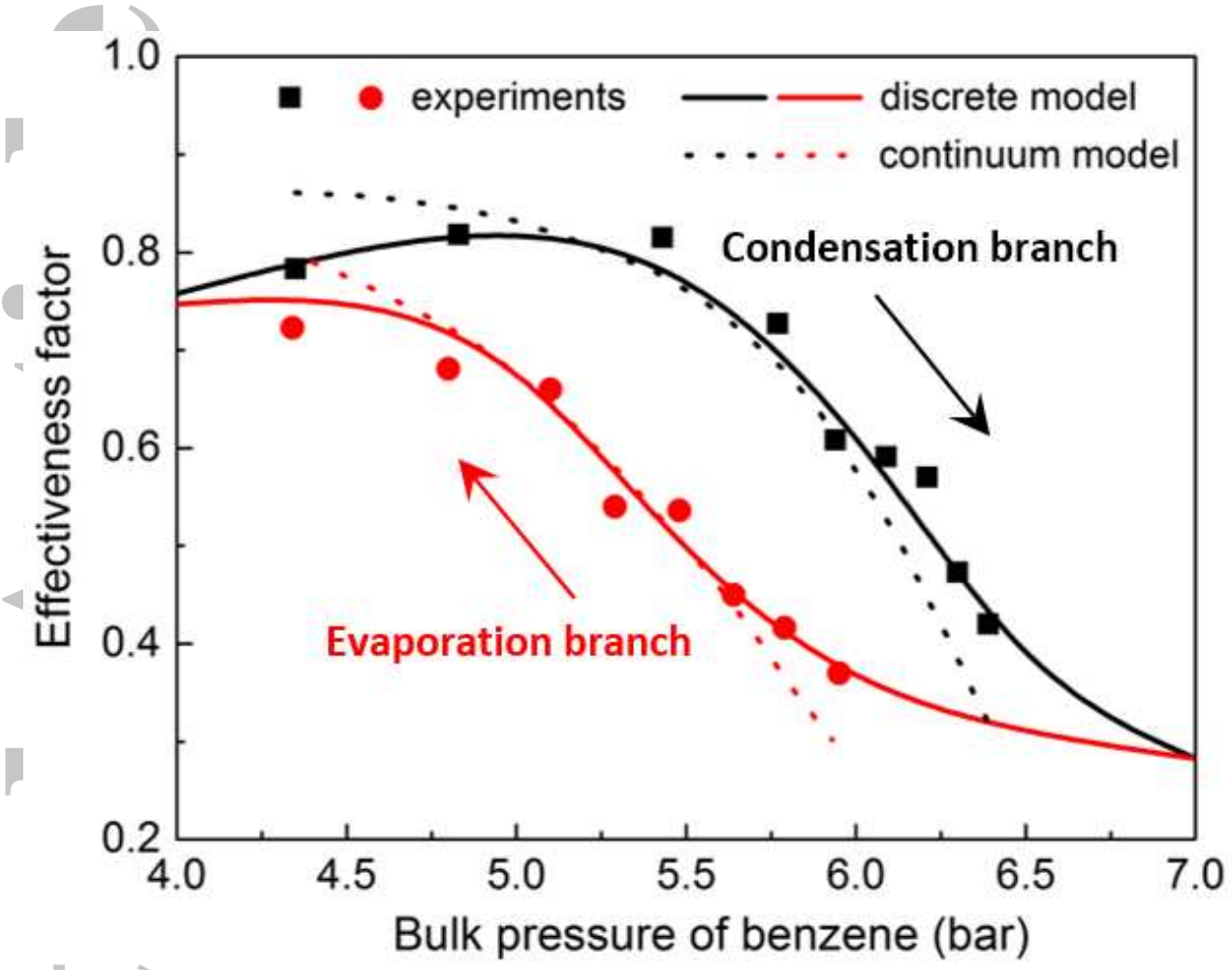

Figure 4. Comparison between the effectiveness factors predicted by the proposed discrete model, the continuum model[4], and experiments[4]. The arrows indicate the direction of changing the bulk pressure of benzene.

Accept

This article is protected by copyright. All rights reserved.

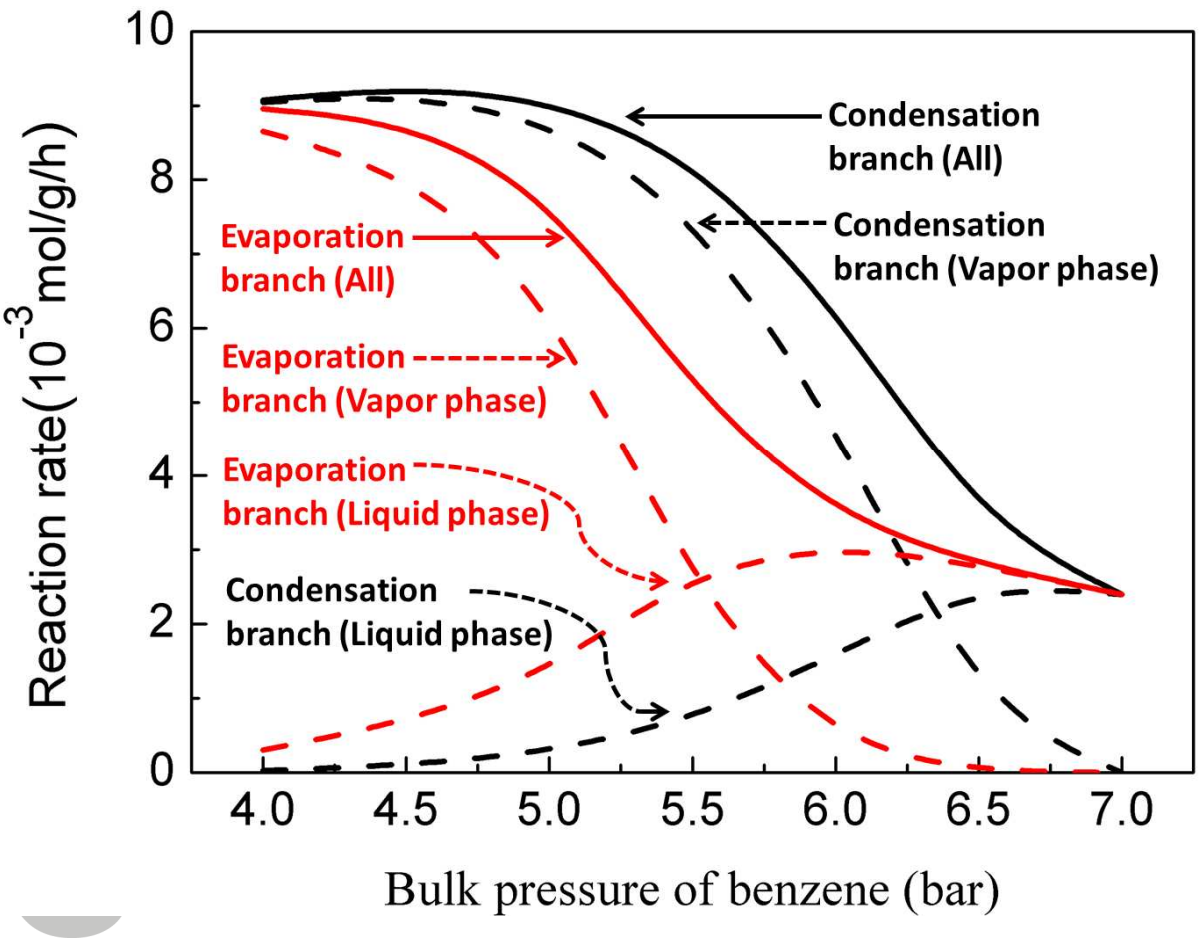

Figure 5. Reaction rates of all pores, vapor-filled pores and liquid-filled pores, as functions of bulk pressure of benzene. The parameters for simulations are presented in Table 1.

Accepted

This article is protected by copyright. All rights reserved.

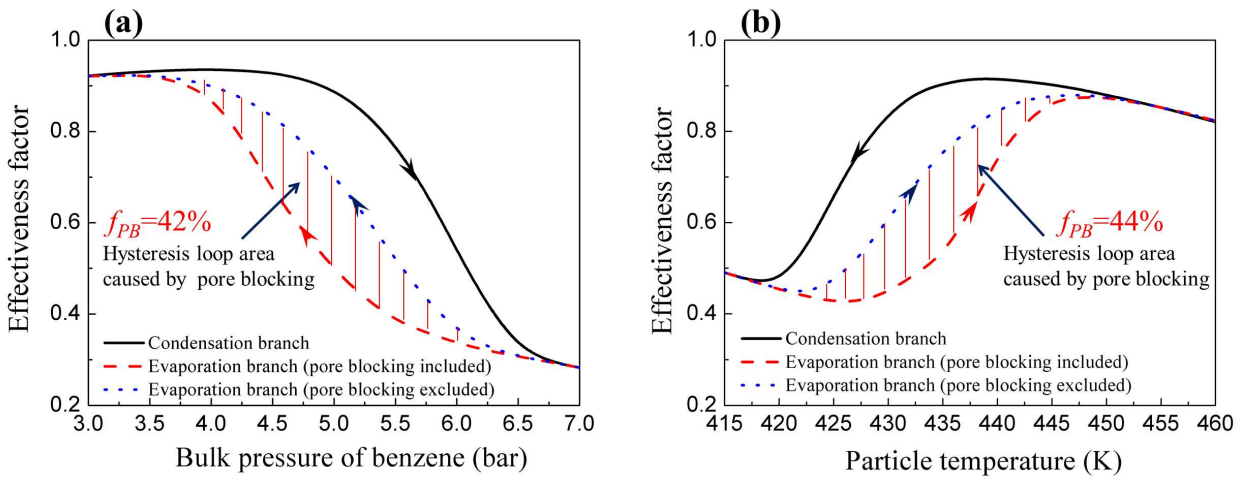

Figure 6. Illustrations of the percentage of the hysteresis loop area caused by pore blocking effects: The effectiveness factor as a function of (a) bulk pressure of benzene and (b) particle temperature. The arrows indicate the direction of a change in bulk pressure of benzene or a change in particle temperature. Fixed parameters: (a) T=433 K, Z=3, r_a=3.5 nm, and σ=0.38; (b) $P_{B,b}$=5 bar, Z=3, r_a=3.5 nm, and σ=0.38.

Accepted

This article is protected by copyright. All rights reserved.

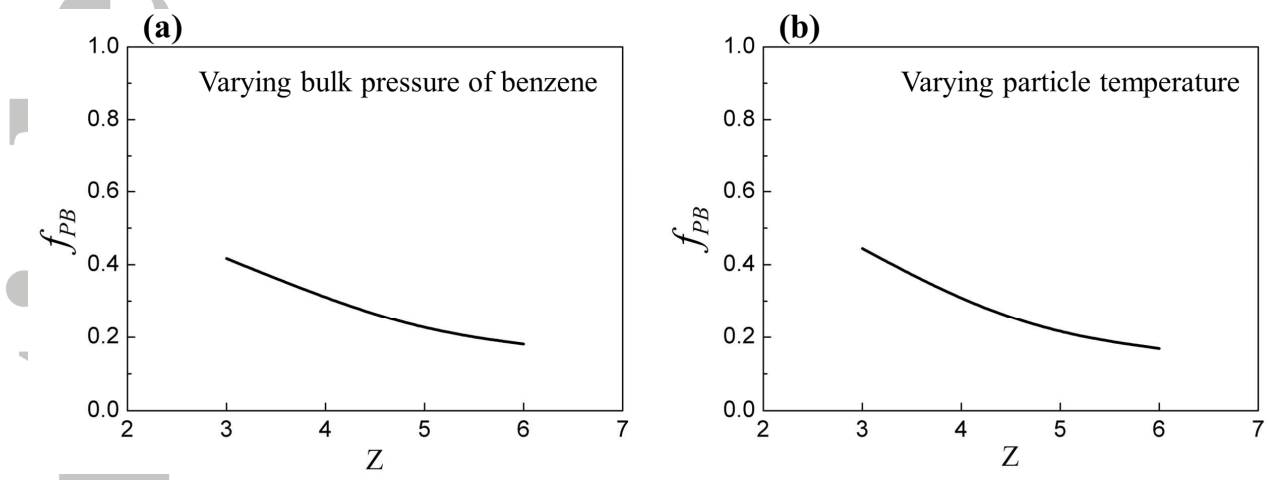

Figure 7. The proportion of the hysteresis loop area caused by pore blocking (f_{PB}) as a function of connectivity (Z). Fixed parameters: (a) T=433 K, r_a=3.5 nm, and σ=0.38; (b) $P_{B,b}$=5 bar, r_a=3.5 nm, and σ=0.38.

Accepted AI

This article is protected by copyright. All rights reserved.

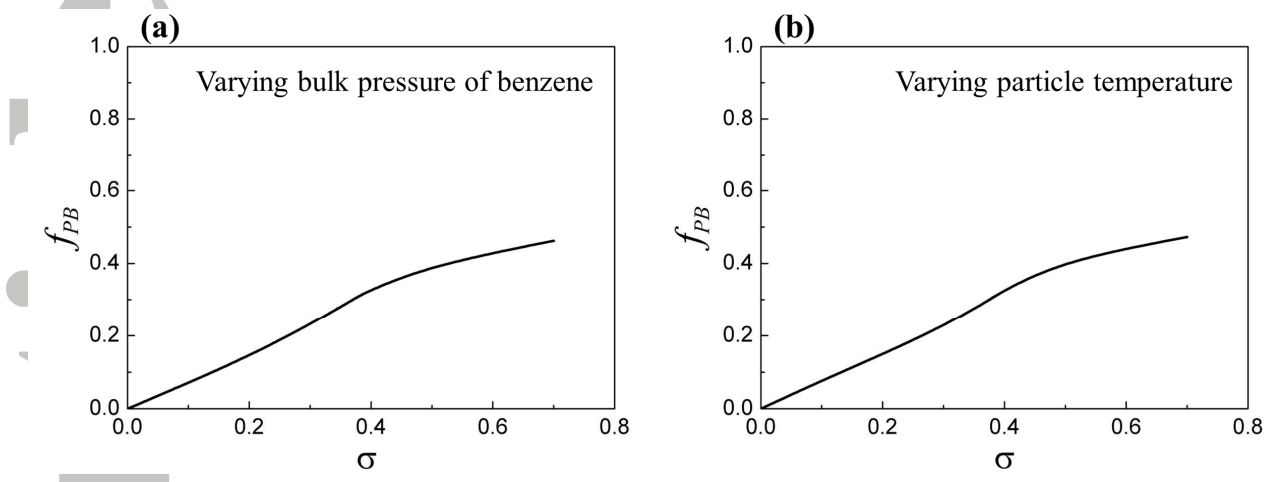

Figure 8. The proportion of the hysteresis loop area caused by pore blocking (f_{PB}) as a function of the standard deviation (σ) of the PSD described by Eq. (1). Fixed parameters: (a) T=433 K, Z=4, and r_a=3.5 nm; (b) $P_{B,b}$=5 bar, Z=4, and r_a=3.5 nm.

Accepted AJ

This article is protected by copyright. All rights reserved.

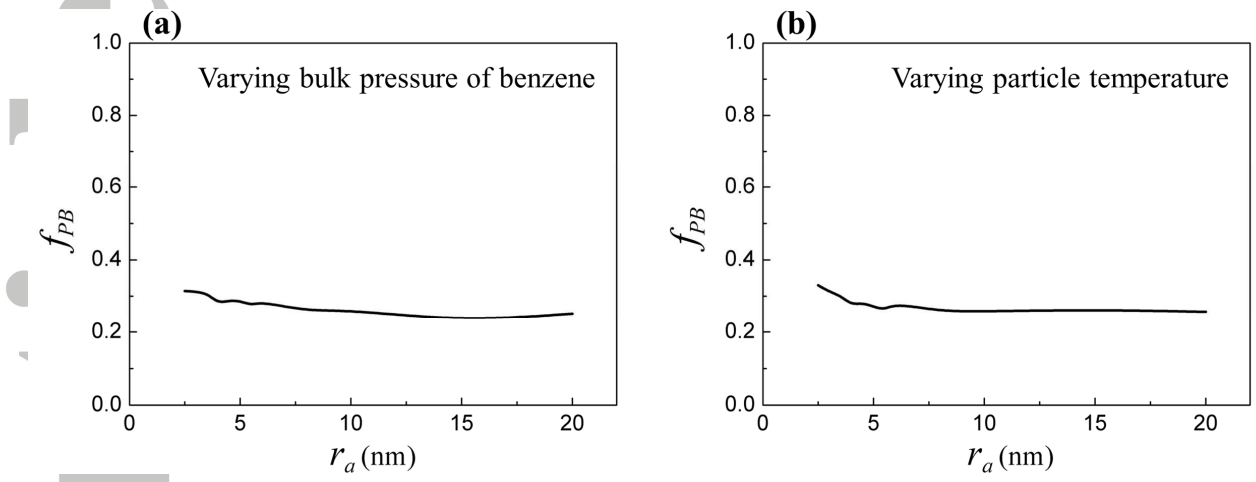

Figure 9. The proportion of the hysteresis loop area caused by pore blocking (f_{PB}) as a function of the volume-averaged pore radius (r_a) of the PSD described by Eq. (1). Fixed parameters: (a) T=433 K, Z=4, and σ=0.38; (b) $P_{B,b}$=5 bar, Z=4, and σ=0.38.

Accepted AIChE

This article is protected by copyright. All rights reserved.

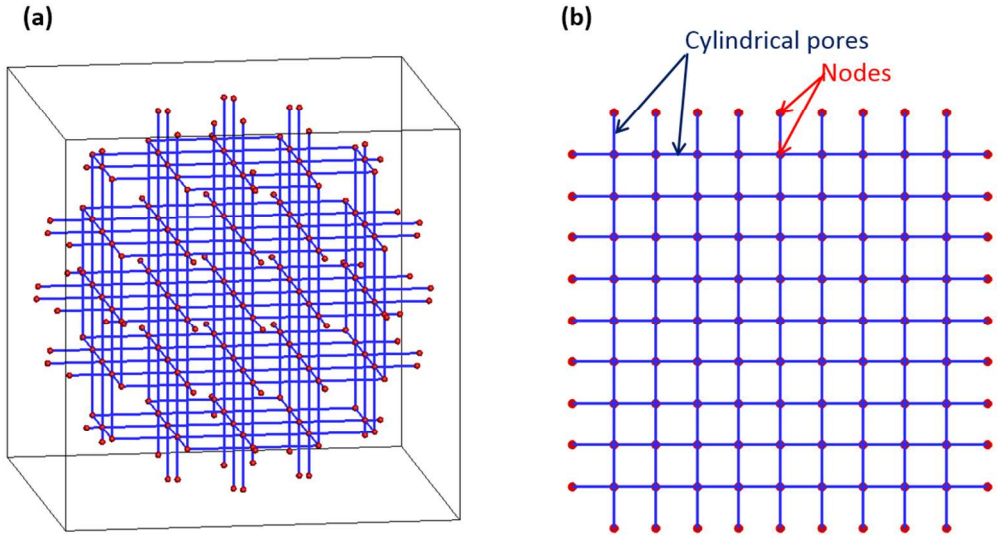

Figure 1. (a) Illustration of three-dimensional pore networks (connectivity=6); (b) illustration of two-dimensional square pore networks (connectivity=4).
427x228mm (72 x 72 DPI)

Accepted

This article is protected by copyright. All rights reserved.

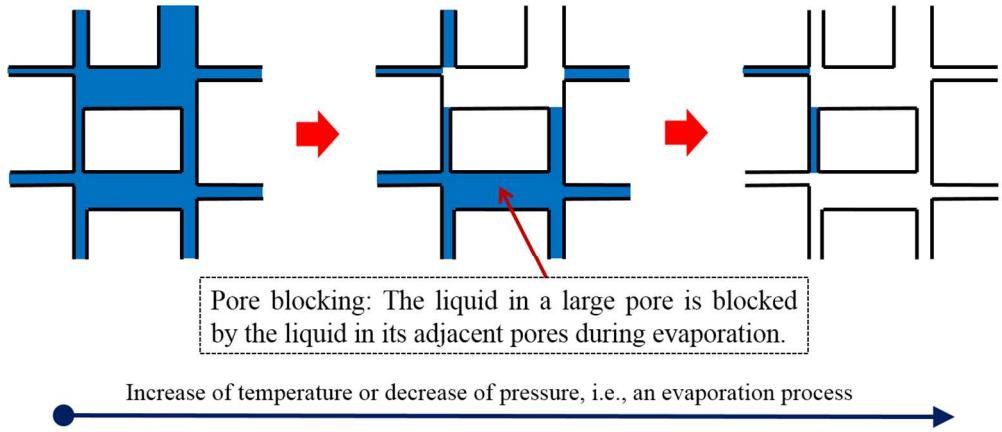

Figure 2. Illustration of the pore blocking phenomenon in the pore network during the evaporation process.
490x212mm (72 x 72 DPI)

Accepted

This article is protected by copyright. All rights reserved.

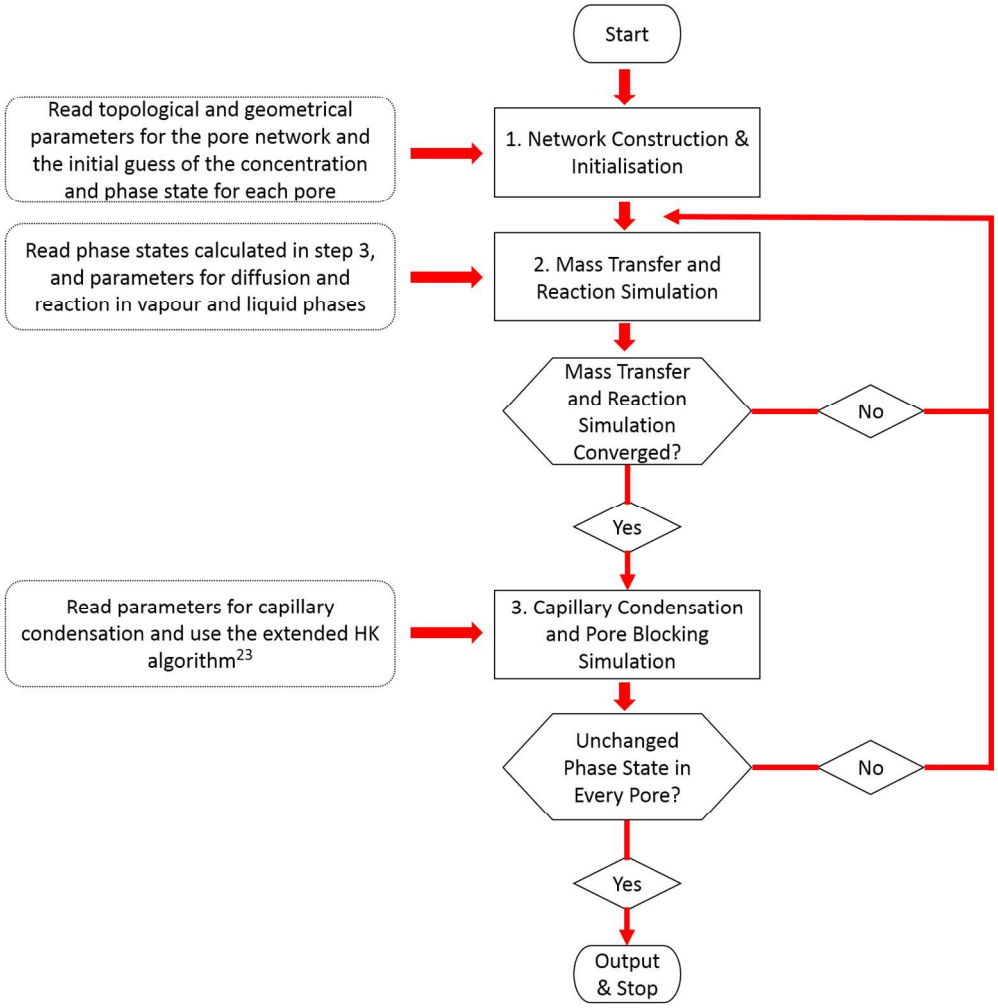

Figure 3. The overall algorithm for the proposed discrete model simulating coupled diffusion, reaction and phase change in porous catalyst particles.
588x599mm (72 x 72 DPI)

This article is protected by copyright. All rights reserved.

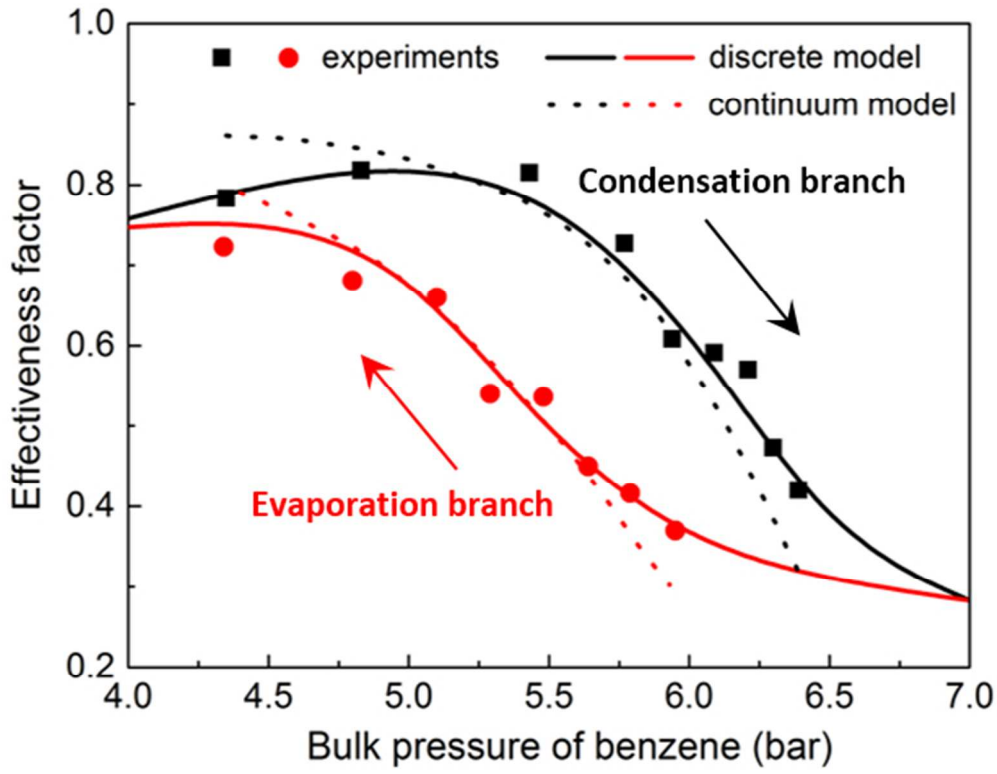

Figure 4. Comparison between the effectiveness factors predicted by the proposed discrete model, the continuum model[4], and experiments[4]. The arrows indicate the direction of changing the bulk pressure of benzene.
104x80mm (150 x 150 DPI)

Accepted

This article is protected by copyright. All rights reserved.

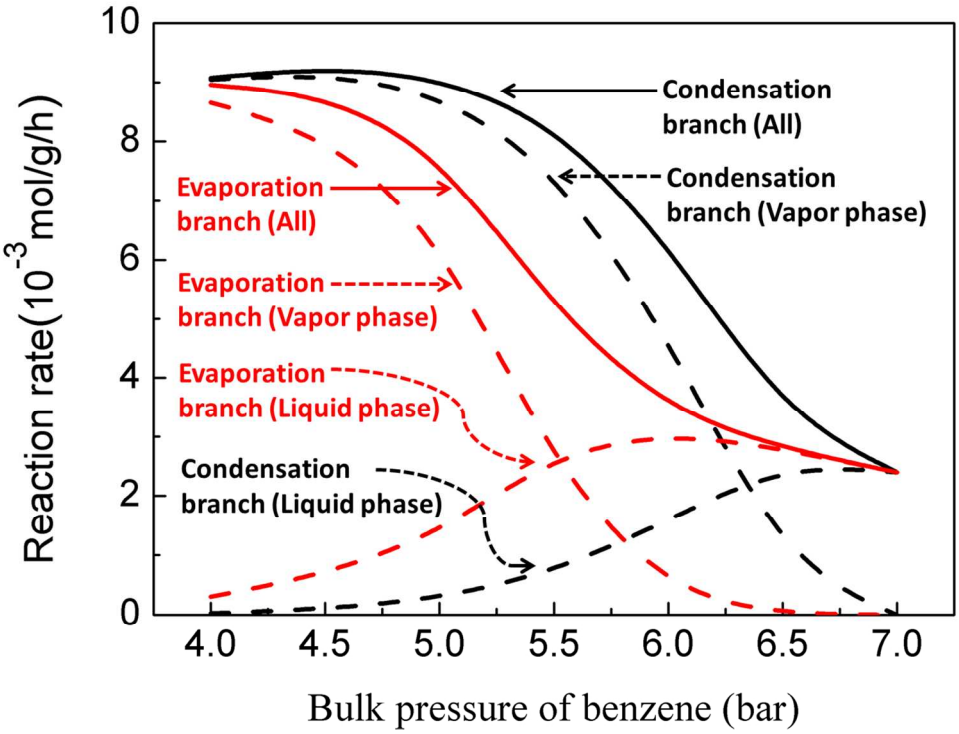

Figure 5. Reaction rates of all pores, vapor-filled pores and liquid-filled pores, as functions of bulk pressure of benzene. The parameters for simulations are presented in Table 1.
241x179mm (150 x 150 DPI)

Accept

This article is protected by copyright. All rights reserved.

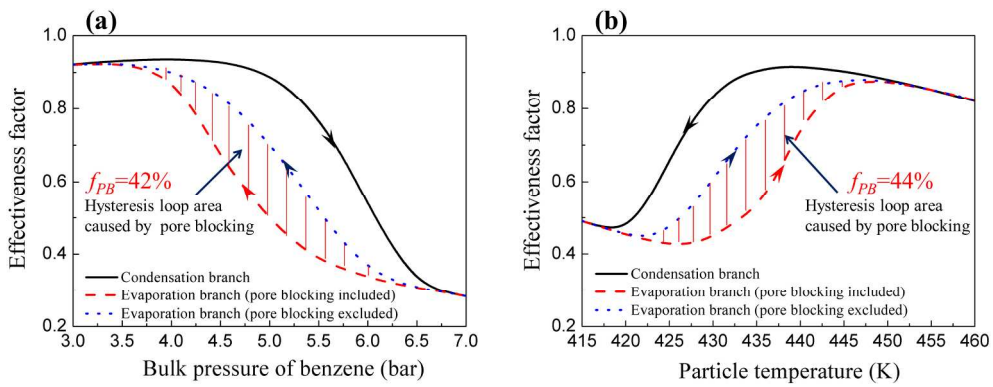

Figure 6. Illustrations of the percentage of the hysteresis loop area caused by pore blocking effects: The effectiveness factor as a function of (a) bulk pressure of benzene and (b) particle temperature. The arrows indicate the direction of a change in bulk pressure of benzene or a change in particle temperature. Fixed parameters: (a) T=433 K, Z=3, r_a=3.5 nm, and σ=0.38; (b) $P_{B,b}$=5 bar, Z=3, r_a=3.5 nm, and σ=0.38.
868x333mm (72 x 72 DPI)

Accepted

This article is protected by copyright. All rights reserved.

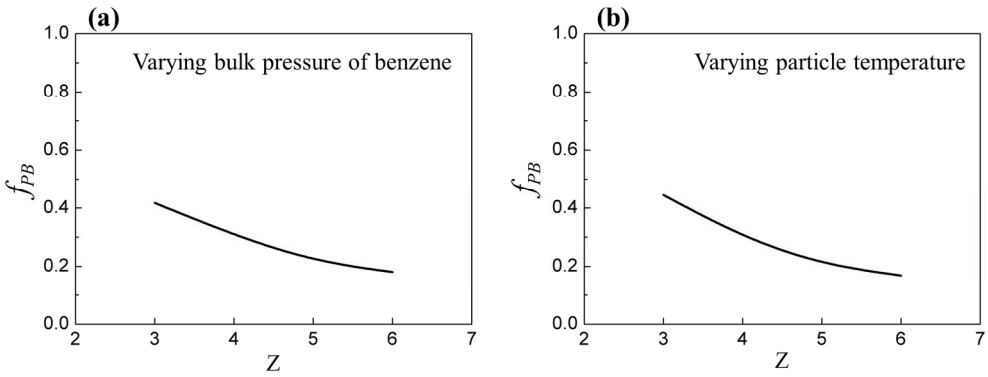

Figure 7. The proportion of the hysteresis loop area caused by pore blocking (f_{PB}) as a function of connectivity (Z). Fixed parameters: (a) T=433 K, r_a=3.5 nm, and σ=0.38; (b) $P_{B,b}$=5 bar, r_a=3.5 nm, and σ=0.38.
875x325mm (72 x 72 DPI)

Accepted

This article is protected by copyright. All rights reserved.

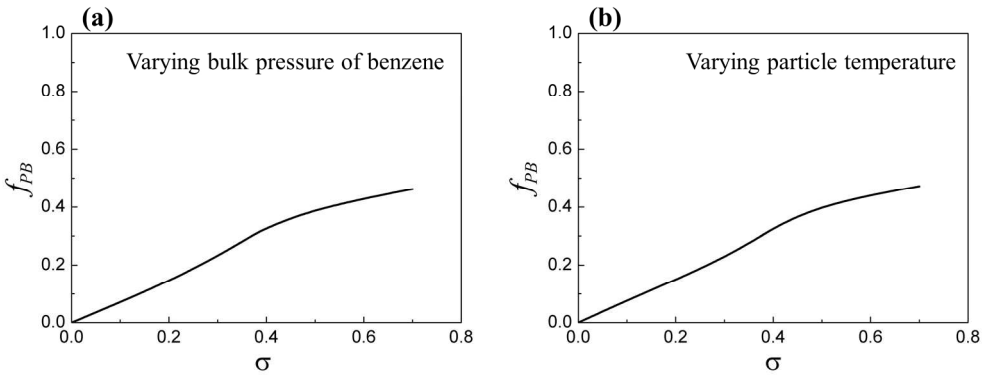

Figure 8. The proportion of the hysteresis loop area caused by pore blocking (f_{PB}) as a function of the standard deviation (σ) of the PSD described by Eq. (1). Fixed parameters: (a) T=433 K, Z=4, and r_a=3.5 nm; (b) $P_{B,b}$=5 bar, Z=4, and r_a=3.5 nm.
875x325mm (72 x 72 DPI)

Accepted Article

This article is protected by copyright. All rights reserved.

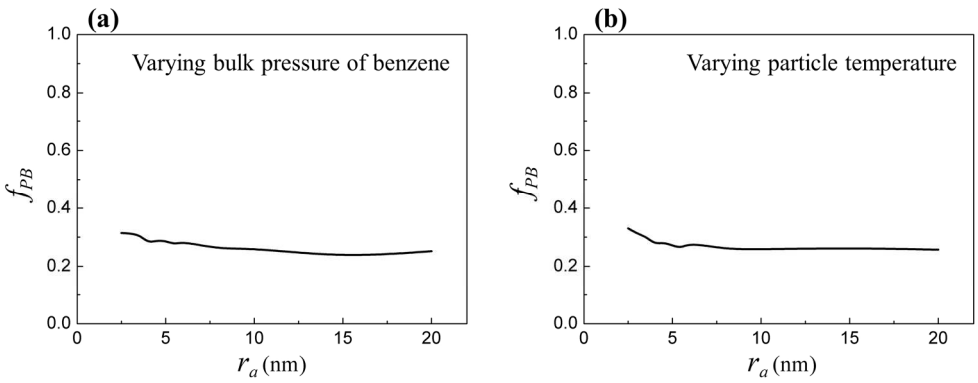

Figure 9. The proportion of the hysteresis loop area caused by pore blocking (f_{PB}) as a function of the volume-averaged pore radius (r_a) of the PSD described by Eq. (1). Fixed parameters: (a) T=433 K, Z=4, and σ=0.38; (b) $P_{B,b}$=5 bar, Z=4, and σ=0.38.
875x325mm (72 x 72 DPI)

Accepted Article

This article is protected by copyright. All rights reserved.